Received: 9 November 2022 | Revised: 3 February 2023 | Accepted: 24 February 2023

DOI: 10.1111/1750-3841.16532

Journal of Food Science WILEY

ORIGINAL ARTICLE

Food Engineering, Materials Science, and Nanotechnology

Semiempirical modeling of a traditional wood-fired pizza oven in quasi-steady-state operating conditions

Aniello Falciano[1] | **Paolo Masi**[1] | **Mauro Moresi**[2]

[1]Department of Agriculture, University of Naples Federico II, Portici, Italy

[2]Department for Innovation in the Biological, Agrofood and Forestry Systems, University of Tuscia, Viterbo, Italy

Correspondence
Mauro Moresi, Department of for Innovation in the Biological, Agrofood and Forestry Systems, University of Tuscia, Viterbo, Italy.
Email: mmoresi@unitus.it

Funding information
Ministero dell'Istruzione, dell'Università e della Ricerca; Italian Ministry of Instruction, University and Research, Grant/Award Number: Special grant PRIN 2017 - prot. 2017SFTX3Y_001

Abstract: Wood-fired ovens are mandatorily used to bake the Neapolitan pizza. Unfortunately, they are still empirically operated. In this work, a pilot-scale wood-fired oven was kept operating in quasi-steady-state conditions. Once the combustion reaction of oak logs had been modeled, the composition of flue gas measured, and the external oven wall and floor temperatures thermographically scanned, it was possible to check for the material and energy balances and, thus, assess that the heat loss rates through flue gas and insulated oven chamber were, respectively, equal to 46% and 26% of the energy supplied by burning firewood. The enthalpy accumulation rate in the internal fire brick oven chamber amounted to about 3.4 kW, this being adequate to keep not only the temperatures of the oven vault and floor practically constant but also to bake one or two pizzas at the same time. Such a rate was predicted by contemplating the simultaneous heat transfer mechanisms of radiation and convection between the oven vault and floor surface areas. The efficacy of the semiempirical modeling developed here was further tested by reconstructing quite accurately the time course of water heating in aluminum trays with a diameter near to that of a typical Neapolitan pizza. The heat flow from the oven vault to the water-containing tray was of the radiative and convective types for about 73% and 15%, whereas the residual 12% was of the conductive type from the oven floor.

KEYWORDS
energy losses through flue gas and insulated oven chamber, energy supplied by wood combustion, material and energy balances, pseudo-steady-state regime performance, thermal efficiency, water heating test, wood-fired pizza oven

Practical Application: Despite wood-fired ovens are largely used in the restaurant and food service industry, their operation is highly dependent on the operator's ability. This study shows how the heat loss rates through flue gas and insulated oven chamber can be assessed, and how the enthalpy accumulation rate in the internal fire brick oven chamber can be predicted by accounting for the simultaneous heat transfer mechanisms of radiation and convection between the

oven vault and floor surface areas. The efficacy of this semi-empirical modelling was further checked for via some water heating tests.

1 | INTRODUCTION

Neapolitan Pizza is a traditional specialty guaranteed by the European Commission Regulation no. 97/2010 (EC, 2010), which is to be baked in wood-fired ovens only. Such equipment is widely used in the restaurant and food service industry all over the world. Nevertheless, it has been very poorly studied so far (Igo et al., 2020; Manhiça, 2014; Manhiça et al., 2012). In contrast, the radiative and convective heat transfer mechanisms in electric pizza ovens were used to describe their performance in steady and unsteady operating conditions by means of three-dimensional numerical models (Ciarmiello & Morrone, 2016a, 2016b).

In previous work (Falciano et al., 2022), the operation of a pilot-scale wood-fired pizza oven was characterized from its start-up phase to its baking operation to provide a basis for future modeling of novel pizza oven design. When baking different white and tomato pizza products, the average thermal efficiency was equal to 13% ± 4% (Falciano et al., 2022).

The operation of a wood-fired oven accounts for four interactive processes: combustion, heat, momentum, and mass transfer. As firewood burns in a specific area of the baking floor, releasing energy and forming the flame, air naturally enters through the open entry door of the oven and makes firewood burn, whereas the resulting flue gas is discharged through the oven chimney. Heat transfer is just one of such processes, and no exact solution can be obtained unless four groups of equations, corresponding to all these processes, are solved simultaneously. In particular, the basic unsteady-state energy equation of heat transfer from the flame to the oven walls and floor must include a mathematical model of heat transfer in the oven, its solution generally being of the numerical type. Strictly speaking, calculations for heat transfer involve semi-theoretical approaches based on experience, especially because certain parameters (i.e., thermal conductivity, thermal diffusivity, diffusion coefficient, viscosity coefficient, and emissivity) are all determined by measurement, during which an accurate relationship between these coefficients and temperature or pressure is mostly unavailable. Empirical methods also attribute uncertainty to one or several factors, including the heat transfer coefficient and thermal effective coefficient. There are zero-, one-, two-, and three-dimensional models available for application to oven heating calculation. In a zero-dimensional model, all physical quantities within the furnace are uniform, and the results are averaged. This method is the one most often used for engineering design (Zhang et al., 2016). One-dimensional models are used to study changes in the physical quantities along the axis (height) of the furnace, where the physical quantity in the perpendicular plane is uniform. This model has practical value for engineering projects such as large-capacity boilers. The two-dimensional model is mainly used for axisymmetric cylindrical furnaces, such as vertical cyclone furnaces (Manhiça et al., 2012). The three-dimensional model describes the furnace process (flow, temperature, chemical species fields, etc.), using three-dimensional coordinates (x, y, and z). In principle, only a three-dimensional model can correctly describe the furnace process. In reality, all the equations used so far for describing the furnace process fail to obtain analytical solutions, and only the numerical methods can reach approximate solutions. Even for an approximate solution, the computational burden is heavy; slow or small-capacity computers are not up to the task. The experience method was previously most applied to zero-dimensional models due to a lack of adequate understanding of the furnace process and related mechanisms. Currently, the semiempirical method is growing in popularity. This method is based on fundamental equations, such as the thermal balance equation and radiative heat transfer equation, as well as certain coefficients or factors obtained through experimentation.

The main aim of this work was to develop a semiempirical model of a wood-fired pizza oven operating in quasi-steady-state conditions. To this end, the first goal was to check for the material and energy balances upon modeling of the combustion reaction of oak logs, measuring the composition of flue gas, and scanning the temperatures of the external oven walls and floor via a thermal imaging camera. The second goal was to estimate the heat losses through flue gas and insulated oven chamber so as to derive the enthalpy accumulation rate in the internal fire brick oven chamber and attempt its mathematical prediction. By analogy with the water boiling tests used to evaluate the energy efficiency of domestic cooking appliances (EC, 2010; Hager & Morawicki, 2013), the third goal was to perform several water heating tests to simulate the water heating profile via the heat transfer mechanisms of radiation, convection, and conduction and, thus, evaluate the net energy transferable to pizza during baking.

FIGURE 1 Picture of the wood-fired pizza oven used in this work.

2 | MATERIALS AND METHODS

2.1 | Equipment

Figure 1 shows a picture of the pilot-scale wood-fired pizza oven used in this work, which was described previously (Falciano et al., 2022). The oven chamber was approximated to a cylinder, having an internal diameter (D_i) and height (H_i) of 90 and 20 cm, respectively, surmounted by an oblate semi-ellipsoidal vault with a height equal to H_i. Thus, the overall volume of the oven chamber was estimated as

$$V_O = \frac{\pi}{4} D_i^2 H_i + \frac{1}{6}\pi D_i^2 H_i = \frac{5}{12}\pi D_i^2 H_i = 0.212\,\mathrm{m}^3 \quad (1)$$

The pizza oven had a semicircular open mouth, its radius being equal to 22 cm. Through its area (S_{OM}), 1 kg of seasoned oak logs every 20 min was fed. Such logs had an average weight, length, diameter, and moisture and ash contents equal to 600 ± 200 g, 250 ± 20 mm, 40 ± 10 mm, and 5.67 ± 0.17 and 2.9% ± 0.7% (w/w), respectively.

As woodfire was burning, the hot combustion flue gas was naturally drawn up and out of the chimney having an internal diameter of 20 cm, whereas ambient air was sucked inside through the open mouth. Its temperature and relative humidity (RH) were measured using a temperature and humidity Mini TH datalogger (XS Instruments, Carpi, MO, Italy). The overall lateral surface area of the internal oven chamber is equal to the lateral surface area of the cylinder mentioned above minus the oven mouth surface area (S_{OM}) plus the lateral surface area of the oblate semi-ellipsoidal vault, the latter being approximated using the following Knud Thomsen formula:

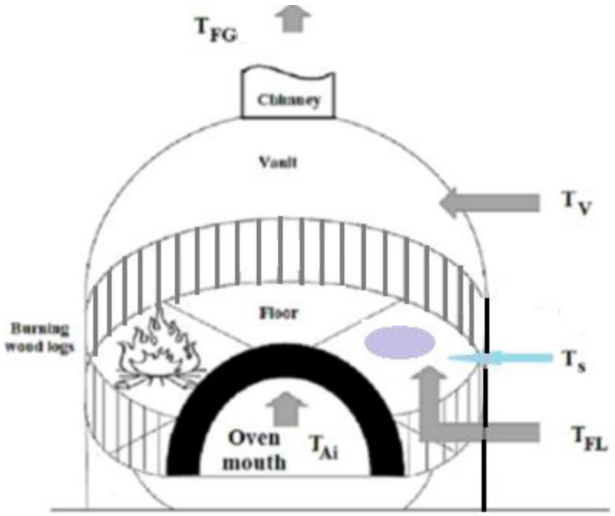

FIGURE 2 Schematic of the wood-fired oven showing the positions of the burning wood logs and sample to be baked, as well the temperatures of input air (T_{Ai}), exit flue gas (T_{FG}), oven floor (T_{FL}) and vault (T_V), and baking sample (T_S).

$$S_{SE} = 2\pi \left[\frac{(a\,b)^p + (a\,c)^p + (b\,c)^p}{3}\right]^{1/p} \quad (2)$$

where a, b, and c are the semiaxes of the ellipsoid, and p (≈1.6075) is an empirical exponent yielding a relative error of at most 1.06%. As in this specific case, $a = b = D_i/2$ and $c = H_i$, the overall lateral surface of the oven chamber was

$$S_{OC} = \pi D_i H_i - S_{OM} + 2\pi \left[\frac{(D_i/2)^{2p} + 2\,(D_i\,H_i/2)^p}{3}\right]^{1/p} = 1.331\,\mathrm{m}^2 \quad (3)$$

Finally, the surface area of the baking floor was

$$S_{FL} = \frac{\pi}{4} D_i^2 = 0.636\,\mathrm{m}^2 \quad (4)$$

The oven walls and floor were about 10 cm in thickness and were made of refractory fire clay bricks, these being characterized by high-temperature resistance, low thermal conductivity, and providing good insulation and high heat accumulation.

Figure 2 shows a schematic of the wood-fired pizza oven showing the positions of the burning wood logs and sample undergoing baking. About one fourth of the floor surface area was occupied by burning wood logs, whereas the remaining surface area was used for pizza baking.

2.2 | Wood-fired pizza oven operation

The start-up procedure for this wood-fired pizza oven, manufactured by MV Napoli Forni (Naples, Italy), was carried out as previously described (Falciano et al., 2022). In this work, the operation of the oven was stabilized by feeding 3 kg of oak logs per hour (Q_{fw}) for about 6 h. The temperatures of the oven vault (T_V) and floor (T_{FL}) were monitored using an infrared (IR) thermal imaging camera (FLIR E95 42°, FLIR System OU, Tallinn, Estonia) equipped with an uncooled microbolometer thermal sensor with dimension 7.888 × 5.916 mm and resolution 464 × 348 pixels, its pixel pitch being 17 μm, focal length of lens 10 mm, and field of view of 42° × 32°. Such temperatures approached the pseudo-steady-state values of 546 ± 53 and 453 ± 32°C, respectively (Falciano et al., 2022). In such conditions, the mean superficial velocity (v_{FG}) and temperature (T_{FG}) of flue gas at the exit section of the oven chimney were simultaneously measured using a Hotwire Anemometer mod RS PRO RS-8880 (RS-Components, Corby, United Kingdom), whereas the flue gas temperature at the oven mouth was determined using the temperature logger 175 T3 (Testo SE & Co. KGaA, Titisee-Neustadt, Germany). Moreover, the dry-bulb temperature (T_A) and RH of ambient air were measured at distances ranging from 0 to 150 cm from the oven entry port using a temperature and humidity Mini TH datalogger (XS Instruments, Carpi, MO, Italy). To check for the aliquot of wood logs combusted during these conditions, as another hour had elapsed from the last log feed, unburned wood logs were separated from wood ashes, weighted, and referred to the overall mass of oak logs supplied, thus yielding the average woodfire combustion efficiency (η_{comb}). The composition of the flue gas exiting from the oven chimney was assessed on 21 April 2022 under meteorological conditions presenting no rain, predominantly calm winds, an ambient temperature of 24.0 ± 0.6°C and pressure of (3.3 ± 0.2 kPa, and good air quality, in accordance with the local air quality standards, as shown in Table 1.

TABLE 1 Chemical composition and flow condition of the flue gas exiting from the chimney of the wood-fired oven operating in quasi-steady-state conditions.

Parameter	Value	Unit
Chimney diameter	200	mm
Chimney cross section	0.0314	m^2
Sampling point below chimney exit	0.7	m
Date	21 April 2022	
Exit temperature	91.1 ± 1.3	°C
Ambient pressure	93.33 ± 0.16	kPa
Ambient temperature	24.0 ± 0.6	°C
Oxygen volumetric fraction	19.8 ± 0.5	% v/v
Moisture volumetric fraction	2.0 ± 0.2	% v/v
CO_2 volumetric fraction	1.4 ± 0.2	% v/v
Average gas velocity	2.9 ± 0.3	m/s
Average gas flow rate	328 ± 43	m^3/h
Average wet gas flow rate	226 ± 30	m^3 (STP)/h
Flue gas molecular mass	28.82 ± 0.03	g/mol
Flue gas density	888 ± 1	g/m^3

2.3 | Water heating tests

Such tests were carried out in triplicate after the oven had been preheated at Q_{fw} = 3 kg/h for 6 h using circular aluminum trays, each one having a diameter of 26 cm and a mass of 19.35 g. Each tray was filled with about 300 g of deionized water at an initial temperature of 25.8 ± 0.2°C, weighted, and then introduced into the oven, where it was kept for 10–80 s. As soon as the tray had been withdrawn from the oven, the temperature of the oven floor was suddenly measured in several areas different from that occupied by the tray using the above thermal imaging camera. Then, the residual mass of the water contained in the tray was measured using an analytical balance (Gibertini, Milan, Italy), whereas its temperature via a temperature logger 175 T3 (Testo SE & Co. KGaA, Titisee-Neustadt, Germany).

2.4 | Statistical analysis of data

Each water heating test was carried out three times. All parameters were shown as average ± standard deviation and were analyzed by the Tukey test at a probability level (p) of 0.05. One-way analysis of variance was carried out using SYSTAT version 8.0 (SPSS Inc., Chicago, IL, USA, 1998).

3 | RESULTS AND DISCUSSION

3.1 | Elemental composition and heating value of oak firewood

Wood is composed of water and dry matter. According to Vassilev et al. (2010), the dry matter of oakwood contains 50.6% carbon (x'_C), 42.9% oxygen (x'_O), 6.1% hydrogen (x'_H), and several other substances, such as 0.3% nitrogen (x'_N), 0.1% sulfur (x'_S), as well as moisture and ash. In this work, the moisture (x_M) and ash (x_A) contents of oak logs

amounted to 5.67 ± 0.17 and 2.89 ± 0.66 g/100 g of wet matter, respectively. Thus, oakwood was characterized by the following raw molecular formula:

$$CH_{1.447}O_{0.636}N_{0.005}S_{0.0007},$$

which is corresponding to a fictitious molecular mass (MM_{fw}) of 23.715 g/mol. Moreover, the higher (HHV) and lower (LHV) heating values were equal to about 18.19 and 16.66 MJ/kg, respectively, as estimated via the following relationships (Mukunda, 2009):

$$HHV = 33.823x'_C + 144.249\left(x'_H - x'_O/8\right) + 9.418x'_S \quad (5)$$

$$LHV = HHV - 22.604x'_H - 2.581x_M \quad (6)$$

where HHV and LHV are expressed in MJ/kg, while x'_i is the weight fraction of the ith element on the dry basis of the biomass under study, and x_M is the moisture content on wet matter.

3.2 | Combustion reaction of oak firewood

Given the dominant influence of fuel-bound nitrogen on NO_X emissions, the NO_X emissions resulting from the combustion of oak firewood were considered the sum of nitrogen monoxide (NO) and nitrogen dioxide (NO_2) and were all expressed as NO_2 equivalents (Ozgen et al., 2021). Thus, the combustion reaction was described as follows:

$$CH_{1.447}O_{0.636}N_{0.005}S_{0.0007} + \alpha O_2 \rightarrow CO_2 + \beta H_2O + \gamma NO_2 + \delta SO_2 \quad (7)$$

where the stoichiometric coefficients α, β, γ, and δ were estimated by writing a material balance for each element of concern, thus obtaining

$$\alpha = 1.050; \beta = 0.723; \gamma = 0.005; \delta = 0.0007.$$

If Q_{fw} is the wet firewood feed rate (expressed in kg/h), its effective molar dry matter combustion rate (R_{fw}) (in kmol/h) would be

$$R_{fw} = \eta_{comb}\frac{(1 - x_M - x_A)}{MM_{fw}}Q_{fw} \quad (8)$$

where the combustion efficiency (η_{comb}) was equal to 87% ± 3%, as determined previously under the aforementioned quasi-steady-state conditions (Falciano et al., 2022).

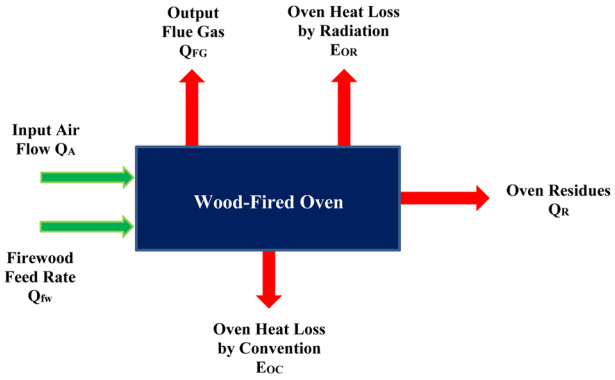

FIGURE 3 Black box model of the wood-fired pizza oven in quasi-steady-state conditions.

Thus, by referring to Equation (7), the weight O_2 consumption and CO_2, NO_2, and SO_2 generation rates were expressed (in kg/h) as follows:

$$r_O = -32\alpha R_{fw} \quad (9)$$

$$r_{CO_2} = 44R_{fw} \quad (10)$$

$$r_{H_2O} = 18\beta R_{fw} \quad (11)$$

$$r_{NO_2} = 46\gamma R_{fw} \quad (12)$$

$$r_{SO_2} = 64\delta R_{fw} \quad (13)$$

Due to woodfire combustion, there is ash and water vapor formation too, with their corresponding weight formation rates being expressed as

$$r_A = \eta_{comb}x_A Q_{fw} \quad (14)$$

$$r_M = \eta_{comb}x_M Q_{fw} \quad (15)$$

3.3 | Black-box modeling of the wood-fired oven

The operation of the wood-fired pizza oven in quasi-steady-state conditions was described by resorting to the black box model shown in Figure 3 to point out simply the functional relationships between system inputs (air and firewood) and system outputs (flue gas, heat dispersion by convention and radiation through the outer surfaces of the oven chamber and floor).

3.3.1 | Material balances of the wood-fired oven

In the circumstances, the overall mass balance yields the following:

$$\left(1 + U_{W,A}\right) Q_A + Q_{\mathrm{fw}} = Q_{\mathrm{FG}} + Q_R \tag{16}$$

with

$$Q_R = (1 - \eta_{\mathrm{comb}}) Q_{\mathrm{fw}} + r_A \tag{17}$$

where Q_R accounts for residues (i.e., unburned logs and wood ash) that cumulate over the oven floor, whereas $U_{W,A}$ is the humidity ratio (in kg of moisture/kg of dry air) of ambient air sucked in through the oven mouth by natural draft.

Provided that dry air (Q_A) consisted of N (76.8% w/w) and O (23.2% w/w), it is possible to write the following partial elemental balances as

$$\mathrm{N}: 0.768\, Q_A = y_{N,\mathrm{FG}} Q_{\mathrm{FG}} \tag{18}$$

$$\mathrm{O_2}: 0.232\, Q_A + r_O = y_{O,\mathrm{FG}} Q_{\mathrm{FG}} \tag{19}$$

$$\mathrm{CO_2}: r_{\mathrm{CO_2}} = y_{\mathrm{CO_2,FG}} Q_{\mathrm{FG}} \tag{20}$$

$$\mathrm{H_2O}: U_{W,A} Q_A + r_{\mathrm{H_2O}} + r_M = y_{\mathrm{H_2O,FG}} Q_{\mathrm{FG}} \tag{21}$$

$$\mathrm{NO_2}: r_{\mathrm{NO_2}} = y_{\mathrm{NO_2,FG}} Q_{\mathrm{FG}} \tag{22}$$

$$\mathrm{SO_2}: r_{\mathrm{SO_2}} = y_{\mathrm{SO_2,FG}} Q_{\mathrm{FG}} \tag{23}$$

where $y_{i,\mathrm{FG}}$ is the weight fraction of the ith component of flue gas.

By summing up all the terms at the left and right sides of Equations (18)–(23), introducing Equations (8)–(15), and accounting for the average values for the moisture (x_M) and ash (x_A) contents and combustion efficiency of oak logs mentioned above, it was possible to relate the input dry air flow rate to the output flue gas rate as

$$Q_{\mathrm{FG}} = Q_A \left(1 + U_{w,A}\right) + r_{\mathrm{O}} + r_{\mathrm{CO_2}} + r_{\mathrm{H_2O}} + r_M + r_{\mathrm{NO_2}} + r_{\mathrm{SO_2}} \cong Q_A \left(1 + U_{w,A}\right) + 0.971 \eta_{\mathrm{comb}} Q_{\mathrm{fw}} \tag{24}$$

To estimate Q_A, the hygrometric properties of ambient air at different distances (d) from the open mouth of the pilot-scale wood-fired pizza oven operating in quasi-steady-state conditions were assessed as shown in Table 2. By resorting to the humidity calculator (available online at https://www.aqua-calc.com/calculate/humidity: accessed on 29 January 2023), it was possible to calculate the corresponding humidity ratio ($U_{W,A}$), as listed in Table 2. Thus, by estimating the flue gas mass flow rate ($Q_{\mathrm{FG}} = 291 \pm 38$ kg/h) from the data listed in Table 1 and assuming the humidity ratio of entering air as coincident with that measured at 50 cm from the oven mouth (Table 2), it was possible to calculate, via Equation (24), the entering dry air mass flow rate ($Q_A = 286 \pm 38$ kg dry air/h). In this way, the estimated molar fractions of O_2 (19.4%), CO_2 (1.0%), and H_2O (2.2%) in the fumes were in good agreement with those experimentally determined (Table 1). Thus, the humidity ratio of flue gas ($U_{W,\mathrm{FG}}$) resulted to be about 13.7 g of water vapor/kg of dry flue gas.

TABLE 2 Hygrometric properties of ambient air at different distances (d) from the open mouth of the pilot-scale wood-fired pizza oven operating in quasi-steady-state conditions.

d (cm)	T_A (°C)	RH (%)	$U_{W,A}$ (g of water vapor/kg of dry air)
0	68.3 ± 3.5	17.2 ± 0.3	35.5 ± 6.4
50	36.4 ± 4.8	20.4 ± 0.9	8.6 ± 2.6
100	24.6 ± 0.8	28.8 ± 1.1	6.0 ± 0.5
150	20.9 ± 0.2	33.1 ± 2.5	5.5 ± 0.5

Abbreviation: RH, relative humidity.

By referring to Equation (7), the theoretical oxygen required to burn 1 kg of oak logs was 2.82 g/g of firewood, whereas the theoretical dry air would be about 12.2 kg/kg of firewood. The effective dry air sucked in through the oven mouth by natural draft was about 95.4 kg/kg of firewood, thus resulting in 682% excess air.

3.3.2 | Heat balance of the wood-fired oven

By referring to the system boundary shown in Figure 3, the heat balance yields the following (Earle & Earle, 1983):

$$e_A Q_A + \eta_{\mathrm{comb}} Q_{\mathrm{fw}} LHV = e_{\mathrm{FG}} Q_{\mathrm{FG},d} + E_{\mathrm{OC}} + E_{\mathrm{OR}} + E_O \tag{25}$$

where η_{comb} and LHV are the firewood combustion efficiency and lower heating value, respectively; E_{OC} and E_{OR} are the energy rate lost by convention and radiation through the external surfaces of the wood-fired oven, whereas E_O is the total enthalpy rate stored in the oven baking chamber made of fire bricks.

The specific enthalpy of input air (e_A) and output flue gas (e_{FG}) on dry mass basis were referred to a standard reference state ($e_R = 0$ for water in the liquid state at 0°C and

ambient pressure) and were calculated as

$$e_A = \left(c_A + U_{w,A} c_{Wv}\right) T_A + U_{W,A} \lambda_{e_0} \quad (26)$$

$$e_{\mathrm{FG}} = \left(c_{\mathrm{FG}} + U_{w,\mathrm{FG}} c_{Wv}\right) T_{\mathrm{FG}} + U_{W,\mathrm{FG}} \lambda_{e_0} \quad (27)$$

where c_A and c_{FG} are the specific heat values of ambient air and flue gas on dry mass basis, whereas c_{Wv} is the specific heat of water vapor and λ_{e_0} is the latent heat of water evaporation at 0°C, respectively.

When the wood-fired oven is operating in quasi-steady-state conditions, its external insulated chamber and floor are generally at higher temperatures than that of ambient air. The resultant air density gradients drive natural or free convection, which is responsible for the energy lost E_{OC}, and can be estimated using the following formula:

$$E_{\mathrm{OC}} = \sum_{i=1}^{n_O} h_{\mathrm{Oi}}\, S_{\mathrm{Oi}} \left(T_{\mathrm{Oi}} - T_A\right) \quad (28)$$

where n_O is the overall number of zones (as identified via IR thermal mapping) of the external oven chamber and floor surface areas, T_{Oi} is the average temperature of the ith zone, S_{Oi} is its surface area, h_{Oi} is the ith convective heat transfer coefficient of ambient air at low-speed flow, and T_A the ambient temperature. In free convection, the dimensionless Nusselt number (Nu):

$$Nu = h_{\mathrm{Oi}} z_i / k_A \quad (29)$$

is a function of the dimensionless Rayleigh number (Ra) and solid shape too:

$$Ra = Gr\, Pr \quad (30)$$

with

$$Gr = (z_i)^3 (\rho_A)^2 g \beta_V \Delta T / (\mu_A)^2 \quad (31)$$

and

$$Pr = c_A \mu A / k_A \quad (32)$$

where Gr and Pr are the Grashof and Prandtl numbers, β_V is the volumetric coefficient of expansion of air (in K^{-1}), ΔT the difference between the temperatures (in °C) of the oven surface (T_{Oi}) and free stream (T_A); g (= 9.81 m^2/s) the acceleration of gravity; c_A, μ_A, ρ_A and k_A are the specific heat, dynamic viscosity, density and thermal conductivity of air at the i-th film temperature (T_{fi}); and z_i is a characteristic dimension of the solid surface (in m).

Table 3 shows all the parameters used to check for the heat balance (Equation 25) of the wood-fired oven examined here, as extracted from Àgueda et al. (2010), Alberti et al. (2018), Anon (n.d.), Choi and Okos (1986), Green and Perry (2008), Henderson-Sellers (1984), Jones et al. (2019), Keyest and Vines (1964), Neutrium (2012), Singh et al. (2009), and The Engineering ToolBox (2003).

As extracted from Alberti et al. (2018), Earle and Earle (1983), and Green and Perry (2008), the functional relationships relating to Nu and Ra for a few solid shapes are listed in Table 4. In this way, the functional relationships related to a cylinder with characteristic dimension $z_i > 1$ m were used to estimate the convective heat transfer coefficients of ambient air contacting each external zone of the oven chamber, whereas those related to a horizontal heated plate facing up or down were used to predict the convective heat transfer coefficient of ambient air contacting the slab supporting pizza or the external floor of the oven.

By using an IR thermal imaging camera, it was possible to scan all the external lateral and frontal surface areas of the oven chamber, as well as that of its external floor and wood embers from the oven entry port, as for instance shown in Figure 4a–d, respectively. In this way, the heat dispersion through the external insulated wall and floor of the pizza oven might be estimated, as well as abnormal temperature mapping might reveal some faults, such as damaged insulation or gaps in the shell, giving rise to heat escape. In this work, all the temperature data collected were automatically grouped into 13 different zones and averaged (Figure 4e), whereas the main dimensions of each zone were assessed using pixel counting, once the measured values of the pixels had been referred to the true dimensions of a few specific distances selected in the external surface areas of the oven. Such dimensions were used to estimate the external surface area of the generic ith zone on the assumption that the oven vault was assimilated to a semi-ellipsoidal solid, whereas the intermediate and inferior parts of the oven to cylinders. All data collected are listed in Table 5 and were used to determine the local heat transfer coefficients h_{Oi} and corresponding heat loss rate (E_{OCi}). The temperature of ambient air was assumed as constant and equal to 24.6°C (Table 2).

The wood-fired oven under study also dissipated some power by radiation (E_{ORi}) from the generic ith external surface area of the oven chamber and floor, including the no-flame and flame areas of the entry port and pizza supporting slab, to ambient air. It can be calculated as

$$E_{\mathrm{OR}} = \sum_{i=1}^{n_O} \varepsilon_i\, \sigma\, S_{Oi} \left(T_{\mathrm{KOi}}^4 - T_{\mathrm{KA}}^4\right) \quad (33)$$

TABLE 3 Parameters used to assess the thermal performance of the wood-fired pizza oven during its quasi-steady-state operation at no-load or during the water heating tests performed in this work.

Parameter	Value	Unit	Refs
Mass of water (m_{W0})	300.0 ± 0.1	g	This work
Mass of aluminum tray (m_V)	19.35 ± 0.05	g	This work
Specific heat of aluminum tray (c_V)	0.890	kJ/(kg K)	Singh et al. (2009)
Density of air (ρ_A)	$358.517\ T_K^{-1.00212}$	kg/m^3	Neutrium (2012)
Specific heat of air (c_A)	$7.875 \times 10^{-6}\ T_K^2 + 0.1712\ T_K + 949.72$	J/(kg K)	Neutrium (2012)
Thermal conductivity of air (k_A)	$-1.3707 \times 10^{-8}\ T_K^2 + 7.616 \times 10^{-5} T_K + 4.5968 \times 10^{-3}$	W/(m K)	Neutrium (2012)
Dynamic viscosity of air (μ_A)	$-8.3123 \times 10^{-12}\ T_K^2 + 4.4156 \times 10^{-8}\ T_K + 6.2299 \times 10^{-6}$	kg/(m s)	Neutrium (2012)
Coefficient of expansion of air (β_{VA})	$1/T_K$	K^{-1}	Neutrium (2012)
Density of water (ρ_W)	$997.18 + 3.144 \times 10^{-3}\ T - 3.7574 \times 10{-}3\ T^2$	kg/m^3	Choi and Okos (1986)
Specific heat of water (c_W)	$4176.2{-}9.0864 \times 10^{-2}\ T + 5.4731 \times 10^{-3}\ T^2$	J/(kg K)	Choi and Okos (1986)
Thermal conductivity of water (k_W)	$0.57109 + 1.7625 \times 10^{-3}\ T - 6.7036 \times 10^{-6}\ T^2$	W/m K	Choi and Okos (1986)
Dynamic viscosity of water (μ_W)	$10/(2.148 \times \{T - 8.435 + \sqrt{[8078.4 + (T - 8.435)^2]}\} - 120)$	Kg/m s	Choi and Okos (1986)
Coefficient of expansion of water (β_{VW})	$81.4 \times 10^{-4} - 4.5/T_K + 647.1142/T_K^2$	K^{-1}	The Engineering ToolBox (2003.)
Latent heat of water evaporation (λ_e)	$1.919 \times 10^3 (\frac{T_S + 273.15}{T_s + 239.24})^2$	kJ/kg	Henderson-Sellers (1984)
Density of water vapor (ρ_v)	$(218.1 \pm 0.4)/T_K$	kg/m^3	Green and Perry (2008, p. 2-414)
Specific heat of water vapor (c_{Wv})	2.08	kJ/(kg K)	Green and Perry (2008, p. 2-414)
Thermal conductivity of water vapor (k_v)	$0.01842 \times (T_K)^{0.5}/(1 + 5485/T_K/10^{(12/TK)})$	W/(m K)	Keyest and Vines (1964)
Dynamic viscosity of water vapor (μ_v)	$\exp[(-4.19 \pm 0.05) + (1.132 \pm 0.007) \times \ln(T_K)] \times 10^{-6}$	kg/(m s)	Green and Perry (2008, p. 2-414)
Density of brick, fireclay (ρ_{FB})	2640	kg/m^3	Green and Perry (2008, p. 2-463)
Specific heat of brick, fireclay (c_{PFB})	0.96	J/(kg K)	Green and Perry (2008, p. 2-463)
Thermal conductivity of brick, fireclay (k_{FB})	1.00	W/(m K)	Green and Perry (2008, p. 2-463)
Emissivity of brick, fireclay (ε_{FB})	$0.9 - 1 \times 10^{-4}\ T_K$	–	Jones et al. (2019)
Emissivity of flame (ε_F)	0.15	–	Àgueda et al. (2010)
Emissivity of ceramic refractory tiles (ε_i)	0.90	–	Anon (n.d.)
Emissivity of polished stainless-steel type 18–8 (ε_i)	0.15	–	Anon (n.d.)
Emissivity of flue gas (ε_G) at $T = 573$°C	0.074	–	Alberti et al. (2018)

where n_O is the overall number of zones identified via IR thermal mapping, ε_i the emissivity of the ith component of the radiating surface area (S_{Oi}), σ ($= 5.67 \times 10^{-8}$ W/(m^2 K^4)) the Stefan–Boltzmann constant, whereas T_{KOi} and T_{KA} are the average absolute temperatures of the ith zone and ambient air. In particular, the emissivity of the flames (ε_F) resulting from oak log combustion was assumed as equal to about 0.15, being their thickness shorter than 0.25 m, as extracted from an experimental study by Àgueda et al. (2010), who observed that only flames thicker than 3.2 m exhibited an emissivity (0.9) close to that of a blackbody, whereas the emissivity of the white ceramic refractory tiles covering the external oven chamber, polished stainless-steel molding, firebrick used for the pizza supporting slab and area surrounding the oven mouth were extracted from Anon (n.d.) and are listed in Table 3. Moreover, the emissivity of hot (gray) gases (ε_G) filling the combustion chamber of the

TABLE 4 Functional relationships relating the dimensionless Nusselt number (*Nu*) to the Rayleigh (*Ra*) number used to estimate the free convective heat transfer coefficient (h_{Oi}) between a free stream and different solid shapes characterized by a linear dimension z_i or between horizontal plates at different temperatures in different flow conditions.

Solid shape	Fluid flow	*Nu* relationship	*Ra* range
Vertical plates and cylinder with $z_i > 1$ m	Fully Laminar	$Nu = 1.36\ Ra^{1/5}$	$Ra < 10^4$
	Laminar	$Nu = 0.55\ Ra^{1/4}$	$10^4 < Ra < 10^9$
	Turbulent	$Nu = 0.13\ Ra^{1/3}$	$Ra > 10^9$
Horizontal heated plates facing up	Laminar	$Nu = 0.54\ Ra^{1/4}$	$1 \times 10^5 < Ra < 2 \times 10^7$
	Turbulent	$Nu = 0.14\ Ra^{1/3}$	$2 \times 10^7 < Ra < 3 \times 10^{10}$
Horizontal heated plates facing down	Laminar	$Nu = 0.27\ Ra^{1/4}$	$3 \times 10^5 < Ra < 3 \times 10^{10}$
Horizontal rectangular cavity	Laminar	$Nu = 0.069\ Ra^{1/3}\ Pr^{0.074}$	$3 \times 10^5 < Ra < 7 \times 10^9$

Source: Extracted from Earle and Earle (1983) and Green and Perry (2008).

wood-fired oven, as viewed from the open oven mouth, was estimated as follows (Alberti et al., 2018):

$$\varepsilon_G = \varepsilon_{H_2O} + \varepsilon_{CO_2} - \Delta \in_{CO_2}^{H_2O} + \Delta \in \quad (34)$$

The single absorbing gas emissivity of species j generally depends on absolute temperature T_K, total pressure P, molar fractions of both the absorbing (x_j) and non-absorbing species (typically N_2), and optical path length L. This emissivity is calculated as if each gas (i.e., H_2O and CO_2) were to be the only radiatively active species in the mixture. Then, the binary overlap correction $\Delta \in_{CO_2}^{H_2O}$ accounts for the band overlapping of such gas species and generally depends on temperature T_K, total pressure P, molar fractions of both the absorbing and the non-absorbing species, and optical path length L. Such data allowed the evaluation of the emissivity of a hemispherical volume of gas, as measured by a small surface element positioned in the center of the hemisphere, its radius representing the optical path length L. Thus, the gas emissivity at the average temperature of the no-flame zone of the oven mouth (zone no. 12 in Table 5) was estimated by assuming that the hemispherical gas volume coincided with the oven volume (V_O), this involving that L was equal to

$$L = \sqrt[3]{\frac{3\ V_O}{4\ \pi}} = 0.37\ \text{m} \quad (35)$$

By using the emissivity data shown in Table 3 and the geometric dimensions of each *i*th zone listed in Table 5, the use of Equations (33)–(35) allowed the *i*th heat loss rate by radiation (E_{ORi}) to be estimated, as reported in Table 5.

Table 6 summarizes the heat balance of the wood-fired pizza oven operating in quasi-steady-state conditions. It can be noted that 46% of the power supplied by firewood is lost through flue gas, whereas 15% and 11% are lost by radiation and convection from the outer surface of the oven walls and floor to the surroundings, respectively. Thus, the energy accumulation rate (E_O), which is stored within the fire brick oven chamber, represented about 28% of the oak log combustion power.

3.3.3 | Heat transfer modes within the wood-fired oven chamber

As firewood was kept burning in quasi-steady-state conditions, the aforementioned energy accumulation rate (E_O) in the oven chamber allowed the temperatures of the internal oven vault (T_V) and floor (T_{FL}) to be maintained approximately constant at 546 ± 53 and 453 ± 32°C, respectively, as reported previously (Falciano et al., 2022). Such heat rate was computed as suggested by Kern (1950), the surface of the oven floor free of oak log burning ($S_{FL'}$) being smaller than the projected enclosing vault area (that coincided with the overall floor area, S_{FL}):

$$E_O = S_{FL'} \frac{1}{\frac{1}{\varepsilon_V} + \frac{S_{FL'}}{S_{FL}}\left(\frac{1}{\varepsilon_{FL}} - 1\right)} \sigma \left(T_V^4 - T_{FL}^4\right) + h_c\ S_{FL'}\ (T_V - T_{FL}) \quad (36)$$

where the total normal emissivity of refractory bricks used for the oven vault and floor was assumed as a linear decreasing function of their absolute temperature in accordance with Jones et al. (2019), as shown in Table 3. Moreover, the convective heat transfer coefficient (h_C) of hot burnt gases contacting the internal vault and baking floor of the oven was estimated using the correlation relative to a horizontal rectangular cavity (Green & Perry, 2008), as listed in Table 4.

In the circumstances, the energy accumulation rate (E_O) estimated by using Equation (36) was just 5% greater than that estimated by the heat balance of the wood-fired oven (Equation 25) and was mainly due to radiation, as shown in Table 6.

TABLE 5 Main dimensions (upper, b_i, and lower, B_i, chord lengths, height, h_i, and surface area, S_{Oi}) and average temperature (T_{Oi}) of the generic *i*th thermally mapped zone of the external chamber and floor of the wood-fired oven operating in quasi-steady-state conditions and calculated parameters (i.e., z_i, T_{fi}, ΔT_i, Pr_i, Ra_i, Nu_i, h_{Oi}) used to evaluate the generic *i*th heat loss rate by convention (E_{OCi}) and radiation (E_{ORi}).

Oven parts	Zone no.	T_{Oi} (°C)	b_i (cm)	B_i (cm)	h_i (cm)	S_{Oi} (cm^2)	z_i (m)	T_{fi} (°C)	ΔT_i (°C)	Pr_i (–)	Ra_i (–)	Nu_i (–)	h_{Oi} (W/(m^2 K))	E_{OCi} (W)	E_{ORi} (W)
Lateral scanning															
Semi-ellipsoidal vault	1	40.2 ± 5.2	31	58	8.8	1282	0.45	32	15.6	0.71	1.18×10^8	57	3.4	6.9	11.8
	2	34.4 ± 4.9	58	94	13.6	3256	0.76	30	9.8	0.72	3.85×10^8	77	2.7	8.5	18.2
	3	33.5 ± 4.2	94	160	25.6	10,525	1.27	29	8.9	0.72	1.64×10^9	153	3.2	29.8	53.3
	4	39.2 ± 4.4	160	193	28.7	10,450	1.77	32	14.6	0.71	6.94×10^9	248	3.7	56.9	89.4
Middle cylinder	5	54.4 ± 6.5	151	151	9.75	2305	1.51	40	29.8	0.71	7.89×10^9	259	4.7	32.0	43.4
	6	61.7 ± 4.7	151	151	18.0	4255	1.51	43	37.1	0.71	9.34×10^9	274	5.0	78.4	103.4
Lower cylinder	7	48.6 ± 2.8	166	166	11.2	2912	1.66	37	24	0.71	8.80×10^9	268	4.4	30.5	42.9
	8	48.1 ± 3.6	166	166	7.5	1950	1.66	36	23.5	0.71	8.65×10^9	267	4.3	19.8	28.1
Oven metal molding	9	41.2 ± 13.7	68	68	5	1227	1.93	33	16.6	0.71	1.02×10^{10}	282	3.9	7.9	2.0
Pizza supporting slab	10	101 ± 51	–	78	24.5	1501	0.51	63	76.4	0.71	5.84×10^8	117	6.5	75.0	75.7
Frontal scanning															
Semi-ellipsoidal vault	1	52 ± 2	31	58	8.8	1282	0.45	38	27	0.71	1.91×10^8	65	3.9	13.8	21.9
	2	50.5 ± 2.4	58	94	13.6	3256	0.76	38	26	0.71	9.08×10^8	95	3.4	28.5	52.3
	3	48.7 ± 4.1	94	160	25.6	10,525	1.27	37	24	0.71	3.99×10^9	206	4.4	110.7	155.8
	4	51.1 ± 8.1	160	193	28.7	10,450	1.77	38	27	0.71	1.16×10^{10}	294	4.5	124.4	172.1
Middle cylinder	5	72.9 ± 12.8	151	151	9.75	1195	1.51	49	48	0.71	1.13×10^{10}	291	5.4	30.9	39.9
	6	71.2 ± 10.8	151	151	18	3145	1.51	48	47	0.71	1.10×10^{10}	289	5.3	77.8	100.6
Oven mouth: flame area	11	654.9 ± 3.4	–	44	22	304	0.44	340	630	0.69	2.17×10^8	67	7.0	134.2	191.8
Oven mouth: no-flame area	12	573 ± 68	–	44	22	456	0.44	299	548	0.69	2.56×10^8	70	6.9	172.7	97.6
Area round the oven mouth	13	187 ± 52	–	80	27.8	1460	0.80	106	162	0.70	2.78×10^9	183	7.2	170.0	230.7
Lower cylinder	7	72.9 ± 12.8	166	166	11.2	2912	1.66	49	48	0.71	8.80×10^9	320	5.4	75.4	97.3
	8	50.3 ± 5.4	166	166	7.5	1950	1.66	37	26	0.71	8.65×10^9	274	4.5	22.3	31.0
Down up scanning															
External oven floor	14	48.7 ± 3.4	–	1.16	–	10,549	1.66	36.7	24.1	0.71	3.03×10^9	63	1.5	37.4	130.1

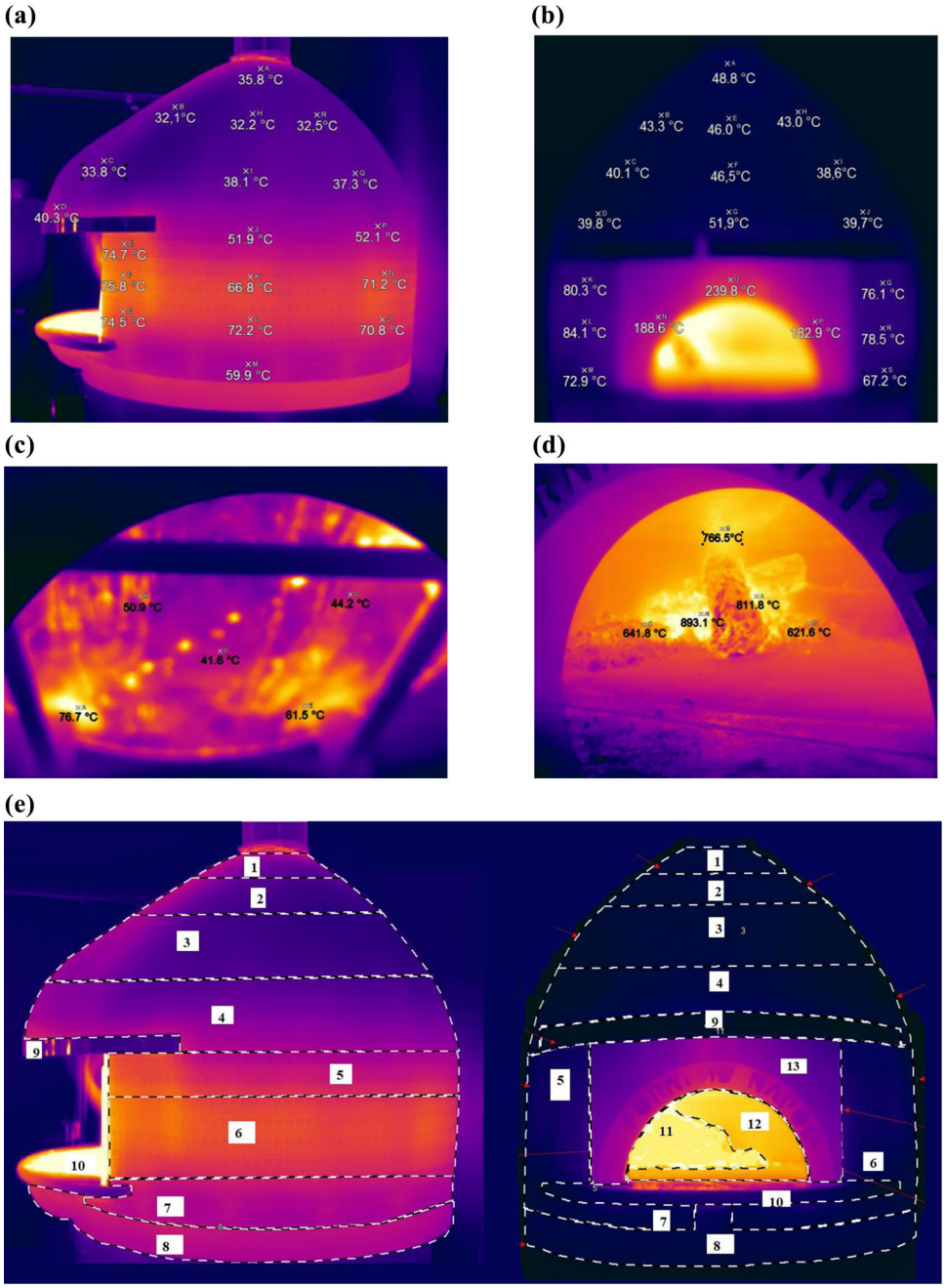

FIGURE 4 Thermal scanning of the external lateral (a), frontal (b), and lower (c) surface areas and entry port (d) of the wood-fired pizza oven operating in quasi-steady-state conditions as such (a–d) and after attributing the temperature data collected to 13 zones of different surface areas and assessing their temperatures in terms of mean value and standard deviation (e).

3.4 | Simulation of the performance of the wood-fired oven via water heating tests

The wood-fired oven was thus characterized by an almost constant energy accumulation rate (E_O) when operating in quasi-steady-state conditions. As an aluminum circular tray filled with deionized water was introduced into the oven chamber, the temperature of the oven vault remained practically unaltered. Similarly, the temperature of the oven floor, as measured at different radial distances larger than 5 cm around each circular tray, was nearly constant. On the contrary, the temperature of the floor area occupied by the sample tended to reduce for a couple of reasons. First, the sample of concern shielded such area from the oven vault irradiation. Second, such floor area tended to cool as heat transferred from it to the cooler sample, the upper side of which was still heated by the oven vault via the heat mechanisms of radiation and free convection

TABLE 6 Main items of the heat balance of the wood-fired pizza oven operating in quasi-steady-state conditions.

Power items	Value	Unit	%
Power supplied by firewood ($\eta_{comb}\ Q_{fw}\ LHV$)	12,079	W	100
Input air enthalpy rate ($e_A\ Q_A$)	*4658*	W	
Output flue gas enthalpy rate ($e_{FG}\ Q_{FG}$)	*10,198*	W	
Heat loss rate through flue gas ($e_{FG}\ Q_{FG}$–$e_A\ Q_A$)	5540	W	46
Heat loss rate to the surroundings by radiation (E_{OR})	1790	W	15
Heat loss rate to the surroundings by convection (E_{OC})	1344	W	11
Enthalpy accumulation rate within the oven chamber (E_O)	3405	W	28
Estimated power exchanged by radiation from the oven vault and floor	*3488*	W	
Estimated power exchanged by convection from the oven vault and floor	*85*	W	
Overall estimated power exchanged from the oven vault and floor	3573	W	

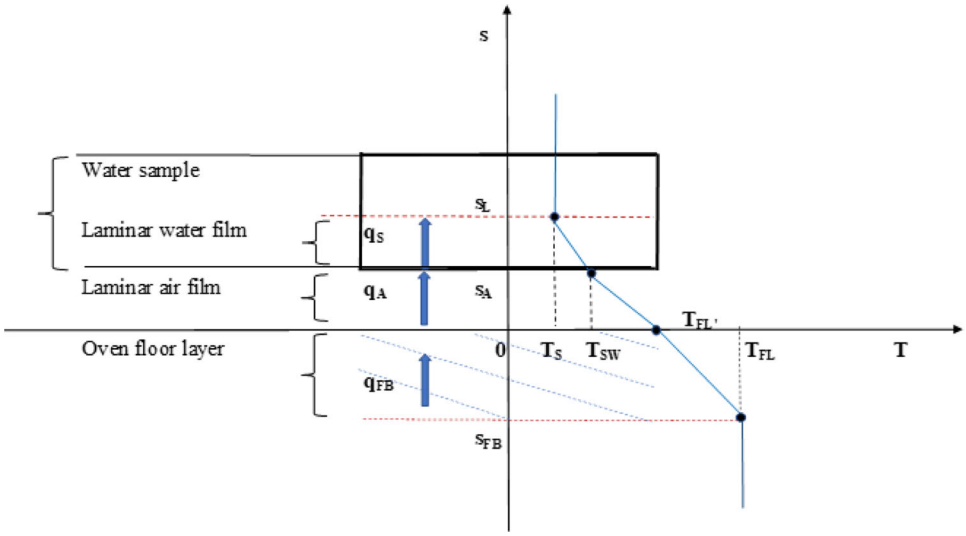

FIGURE 5 Temperature profiles and heat flux through different layers when a water-containing tray is laid over the oven floor at temperature T_{FL}. All symbols are described in the Nomenclature section.

while some of its moisture was also evaporated. In these conditions, the conductive heat process was assumed to be limited to a restricted floor volume, its base coinciding with the area occupied by the tray itself and its thickness (s_{FB}) being of the order of a few centimeters, respectively. Because the water-containing aluminum tray was not in very intimate contact with the hot oven floor owing to a thin film of hot air, the heat transfer between the tray and oven floor took place largely by natural convection.

Figure 5 shows the temperature profile from the bulk of the oven floor, its temperature (T_{FL}) being almost invariant with respect to the initial value (T_{FL0}), to its upper side ($T_{FL'}$), which was separated from the tray lower side at T_{SW} by a gaseous film and then from T_{SW} to the average water temperature (T_S) in the tray. The instantaneous heat flux through such three laminar layers was assumed to be constant ($q_{cond} = q_{FB} = q_A = q_S$). The heat flux through the laminar water film contacting the lower side of the tray was of the convective type. By assuming the thermal resistance of the aluminum tray as negligible and the oven floor as a semi-infinite solid at a constant initial temperature ($T_{FL} = T_{FL0}$), the heat flux exchanged was expressed as (Carslaw & Jaeger, 1959; Varlamov et al., 2018)

$$\begin{aligned} q_S\ dt &= -h_S\ (T_S - T_{SW})\, dt = q_A\ dt \\ &= -h_A\ \left(T_{SW} - T_{FL'}\right)\ dt = q_{FB}\ dt \\ &= -k_{FB}\ \frac{T_{FL'} - T_{FL}}{\sqrt{\pi\ \alpha_{FB}\ t}} \end{aligned} \tag{37}$$

Such heat flux was then related to the heat balance of the oven floor section covered by the tray itself as

$$q_{FB}\ dt = s_{FB}\ \rho_{FB}\ c_{pFB}\ (-dT_{FL'}) \tag{38}$$

where s_{FB} is the thickness of the oven floor area exhibiting a temperature drop as it contacts the tray initially at room temperature.

By equating the left and central sides of Equation (37), it was possible to express the temperature (T_{SW}) of the lower tray side as follows:

$$T_{SW} = \frac{T_S + \gamma_{AS}\, T_{FL'}}{1 + \gamma_{AS}} \tag{39}$$

with

$$\gamma_{AS} = h_A / h_S \tag{40}$$

By referring to the right and central sides of Equation (37), it was possible to estimate the local floor temperature ($T_{FL'}$) as

$$T_{FL'} = \frac{h_A\, T_{SW}\, \sqrt{\pi\, \alpha_{FB}\, t} + k_{FB}\, T_{FL}}{h_A\, \sqrt{\pi\, \alpha_{FB}\, t} + k_{FB}} \tag{41}$$

By assuming that at the boundary between the tray and oven floor, the instantaneous heat flux ($q_{cond} = q_S = q_A = q_{FB}$) was constant throughout the three laminar layers shown in Figure 5, it was possible to evaluate its time course as

$$q_{cond} = \frac{T_{FL} - T_S}{\frac{1}{h_S} + \frac{1}{h_A} + \frac{\sqrt{\pi\, \alpha_{FB}\, t}}{k_{FB}}} \tag{42}$$

Finally, the heat balance for the water-containing tray fed through the entry port of the wood-fired oven operating in quasi-steady-state conditions may be written as

$$S_S \left[\frac{1}{\frac{1}{\varepsilon_V} + \frac{S_S}{S_{FL}} \left(\frac{1}{\varepsilon_S} - 1 \right)} \sigma \left(T_V^4 - T_S^4 \right) + h_c \left(T_V - T_S \right) + q_{cond} \right]$$

$$dt = \left[m_W(t)\, c_W + m_V\, c_V \right] dT_S + \lambda_e\, dm_e \tag{43}$$

with

$$m_e = m_{W0} - m_W(t) \tag{44}$$

The amount of water evaporated during the water heating tests carried out here was found to be a nonlinear function of the average water temperature (T_S). By plotting the mass of water evaporated (m_e) against T_S using a semilogarithmic plot (Figure 6), it was possible to describe m_e via the following empirical relationship:

$$\ln(m_e) = a_0 + a_1 T_S \tag{45}$$

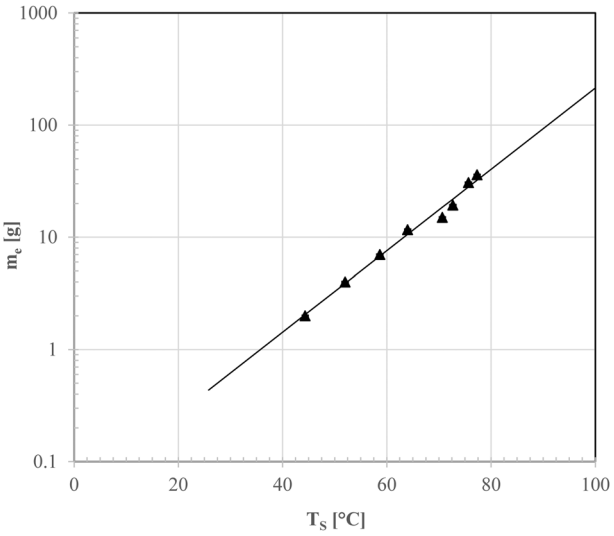

FIGURE 6 Semilogarithmic plot of the amount of water evaporated (m_e) against the average temperature of the water in the tray (T_S: ▲) during the water heating tests, whereas the continuous line was plotted using the least squares regression equation (Equation 45) with the coefficients reported in the text.

where a_0 and a_1 are empirical coefficients that can be determined by fitting [ln(m_e)-vs.-T_S] data via the method of least squares:

$a_0 = -2.99 \pm 0.26$; $a_1 = 0.084 \pm 0.004\,°C^{-1}$ ($r^2 = 0.987$).

In this way, the derivate of m_e with respect to time may be expressed as

$$\frac{dm_e}{dt} = a_1\, e^{a_0 + a_1 T_S} \frac{dT_S}{dt} = a_1\, m_e \frac{dT_S}{dt} \tag{46}$$

In conclusion, once Equation (46) had been introduced into Equation (43), it was possible to reconstruct the time course of T_S by integrating numerically the following first-order differential equation:

$$\frac{dT_S}{dt} = \frac{S_S}{m_W(t)\, c_W + m_V\, c_V + \lambda_e\, a_1\, m_e} \left[\frac{\sigma}{\frac{1}{\varepsilon_V} + \frac{S_S}{S_{FL}} \left(\frac{1}{\varepsilon_S} - 1 \right)} \left(T_V^4 - T_S^4 \right) + h_c \left(T_V - T_S \right) + q_{cond} \right] \tag{47}$$

with the following initial and boundary conditions:

$$T_S = T_{S0};\ T_{FL'} = T_{FL0};\ m_e = 0 \text{ for } t = 0 \tag{48}$$

$$T_V = T_{V0};\ T_{FL} = T_{FL0} \text{ for } t \geq 0 \tag{49}$$

and the physical constraints expressing the amount of water evaporated (Equation 45), the temperatures of the tray (T_{SW}) and oven floor ($T_{FL'}$) using Equations (39) and (41), and the heat flux (q_{cond}) using Equation (42).

By referring to the above semiempirical model, it was possible to reconstruct the time course of T_S during the aforementioned water heating tests, as reported below.

3.4.1 | Water heating test

As the wood-fired oven had been ignited with 3 kg of oak logs for not shorter than 6 h, several aluminum trays, each one containing 300 g of deionized water, were fed through the oven entry port and heated for times ranging from 0 to 80 s. Although the oven floor temperature was practically constant (448 ± 5°C), the sample temperature (T_S) increased from T_{S0} (25.8 ± 0.2°C) to 77.3 ± 1.2°C, and its mass (m_W) decreased from 300 ± 0 to 264 ± 4 g because of water evaporation.

Because the aluminum tray was just laid upon the hot oven floor, the heat transferred through its base was mainly controlled by the thermal resistance of the gaseous film between both surfaces. In fact, the free convection heat transfer coefficients pertaining to the laminar gaseous (h_A) and water (h_S) films (see Figure 5) resulted to be of the order of 9 and 500 W/(m^2 K^2), respectively, as calculated via the relationships listed in Table 4 for horizontal heated plates facing up with the physical properties of air and water reported in Table 3.

Figure 7 shows the time course of the calculated values of the water mass (m_W) and temperature (T_S), as well as the temperature at the tray base (T_{SW}), and oven floor beneath the tray ($T_{FL'}$) using the mathematical model described in Section 3.4.

It can be noted quite a good reconstruction of the experimental profiles of T_S and m_W. The accuracy of both the calculated profiles was found to be sensitive to the overall heat transfer coefficient h_A. In fact, by increasing it from 9 to 18 W/(m^2 K), the average mean percentage errors between the experimental and calculated T_S and m_W values reduced from 8.1% and 1.8% to 4.1% and 0.8%, respectively.

Thus, according to Equation (43), the overall heat flow to the water contained in an aluminum tray was predominantly represented by radiative heat (72.5% ± 0.9%), followed by convective heat (15.5% ± 0.3%) and conductive heat (12.0% ± 0.6%). Finally, the average power transferred to the water was 1.49 ± 0.03 kW, corresponding to an overall thermal energy of about 118 kJ. Because the energy released by the combustion of 3 kg/h of oaks logs during the time interval of 80 s accounted for amounted to 966.4 kJ, the water heating test in question revealed an energy efficiency near 12.2%. Such average energy efficiency for the pizza oven examined here was greater than that (6%–7%) of gaseous domestic ovens (Cimini & Moresi, 2022; Hager & Morawicki, 2013), but smaller than that estimated for a metal fired-wood oven by Igo et al. (2020). In such cases, the main energy loss was due to the dispersion of hot fumes (Table 6).

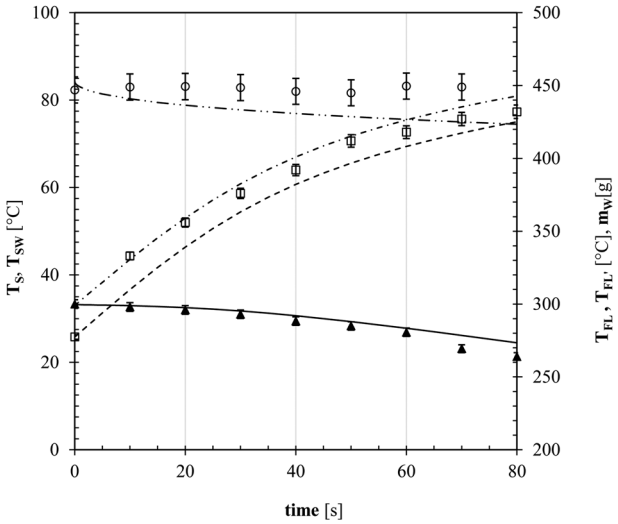

FIGURE 7 Time course of the experimental temperature (T_S: □) and overall mass of water (m_W: △ (closed triangle, not empty one) contained in an aluminum tray, and temperature of the oven floor around the sample itself (T_{FL}: open circle), as well as the calculated values of m_W (continuous line), T_S (broken line), T_{SW} (dash-dotted line), and $T_{FL'}$ (dash-double dotted line) using the mathematical model described in the text.

In previous work (Falciano et al., 2022), it was observed that the average thermal efficiency of this pilot-scale wood-fired oven was 13% ± 4% when referring to either this water heating test or several other baking tests carried with white or tomato pizzas as such or topped with sunflower oil. In the circumstances, the heat collected by the water-containing aluminum circular tray should be regarded as quite near to that collected by any pizza sample with almost the same diameter. Because the enthalpy accumulation rate within the oven fire brick chamber (E_O) in the quasi-steady-state conditions was about 3.4 kW (Table 6) and the water heating tests made use of just 44% of E_O, it would be possible to confirm the nominal baking capacity of two pizzas at once for this wood-fired oven.

4 | CONCLUSIONS

In this work, the material and energy balances in a pilot-scale wood-fired oven in quasi-steady-state operating conditions were established in conjunction with the measurement of the main composition of flue gas and external oven wall and floor temperatures in order to assess the heat

loss rates through flue gas and insulated oven chamber. About 46% and 26% of the energy supplied by firewood combustion were dissipated by the exit fumes and external oven surfaces to the surrounding environment. The remaining 28% accumulated in the internal fire brick oven chamber, thus allowing the temperatures of the oven vault and floor to be kept approximately constant, as well as one or two pizzas to be baked at once. By accounting for the simultaneous heat transfer mechanisms of radiation, convection, and conduction, it was possible to simulate quite accurately a series of water heating tests carried out using water-containing aluminum trays with a diameter near to that of a typical Neapolitan pizza. The overall heat transferred to each pizza-simulating tray was mainly due to radiation (circa 73%), the contribution of the convective heat from the oven vault and conductive heat from the oven floor amounting to about 15% and 12%, respectively.

Further work should be aimed at checking the capability of this semiempirical model to predict the baking process of typical pizzas differently topped.

NOMENCLATURE

a, b, c	semiaxes of the semi-ellipsoid vault (m)
a_0, a_1	empirical coefficients of Equation (45)
b_i, B_i	upper and lower chord lengths of the ith thermally mapped zone of the external oven surface (m)
c_i	specific heat of the ith component or solid (J/kg K)
c_V	specific heat of aluminum tray (J/kg K)
c_W	specific heat of water (J/kg K)
c_{Wv}	specific heat of water vapor (J/kg K)
d	orthogonal distance from the oven mouth (m)
D_i	diameter of the internal oven chamber (m)
e_i	specific enthalpy of ith gaseous stream on dry mass basis (J/kg)
E_O	enthalpy accumulation rate inside the internal fire brick oven chamber (W)
E_{OC}	energy rate lost through the external oven surfaces by convention (W)
E_{OR}	energy rate lost through the external oven surfaces by radiation (W)
e_R	specific enthalpy at the standard reference state (J/kg)
g	acceleration of gravity (= 9.81 m^2/s)
Gr	Grashof number as defined by Equation (31) (dimensionless)
h_A	convective heat transfer coefficient through the laminar gaseous film (W/(m^2 K))
h_c	convective heat transfer coefficient of the gas mixture filling the internal oven chamber (W/(m^2 K))
HHV	higher heating value of firewood (MJ/kg)
h_i	height of the ith thermally mapped zone of the external oven surface (m)
H_i	height of the internal oven chamber (m)
h_{Oi}	convective heat transfer coefficient of ambient air contacting the ith external surface area of the oven chamber (W/(m^2 K))
h_S	convective heat transfer coefficient through the laminar water film (W/(m^2 K))
k_i	thermal conductivity of the ith fluid or solid (W/(m^2 K))
L	optical path length of the gas-emitting gas as defined by Equation (35) (m)
LHV	lower heating value of firewood (MJ/kg)
m_e	mass of water evaporated (kg)
MM_{fw}	molecular mass of firewood (g/mol)
m_V	mass of aluminum tray (kg)
m_W	instantaneous mass of water (kg)
n_O	overall number of thermally mapped zones (dimensionless)
Nu	Nusselt number as defined by Equation (29) (dimensionless)
p	empirical exponent of Knud Thomsen's formula ($p \approx 1.6075$) (dimensionless)
Pr	Prandtl number as defined by Equation (32) (dimensionless)
q_A	instantaneous convective heat flux through the laminar gaseous film (W/m^2)
Q_A	mass flow rate of input dry air (kg/h)
q_{cond}	instantaneous heat flux as defined by Equation (42) (W/m^2)
q_{FB}	instantaneous conductive heat flux through the firebrick layer (W/m^2)
Q_{FG}	mass flow rate of output wet flue gas (kg/h)
Q_{FGd}	mass flow rate of output dry flue gas (kg/h)
Q_{fw}	wet firewood feed rate (kg/h)
Q_R	accumulation rate of solid residues over the oven floor (kg/h)
q_S	instantaneous convective heat flux through the laminar water film (W/m^2)
r^2	coefficient of determination
Ra	Rayleigh number as defined by Equation (30) (dimensionless)
R_{fw}	effective molar dry matter combustion rate (kmol/h)
RH	relative humidity of ambient air (%)
r_i	weight generation or consumption rate of the ith component (kg/h)
s	vertical axis (m)
s_A	thickness of the laminar gaseous film (m)
s_{FB}	thickness of the firebrick layer (m)
S_{FL}	surface area of the oven floor (m^2)
s_L	thickness of the laminar water film (m)

S_{OC} overall lateral surface of the oven chamber (m^2)
S_{Oi} surface area of the ith thermally mapped zone of the oven chamber (m^2)
S_{OM} surface area of the semicircular oven mouth (m^2)
SS surface area of the circular tray (m^2)
S_{SE} lateral surface area of the oblate semi-ellipsoidal vault (m^2)
t baking time (s)
T_A temperature of ambient air (°C)
T_{FG} temperature of flue gas (°C)
T_{fi} temperature of the ith laminar film (°C)
T_{FL} temperature of the oven floor (°C)
$T_{FL'}$ temperature of the oven floor shielded by a tray (°C)
T_{KA} absolute temperature of ambient air (K)
T_{KOi} average absolute temperatures of the ith thermally mapped zone of the oven chamber (K)
T_{Oi} average temperature of the ith thermally mapped zone of the oven chamber (°C)
T_S average temperature of the water contained in the tray (°C)
T_{SW} average temperature of the tray lower side laid over the oven floor (°C)
T_V average absolute temperature of the oven vault in quasi steady-state conditions (K)
$U_{W,A}$ humidity ratio of ambient air (kg of water vapor/kg of dry air)
$U_{W,FG}$ humidity ratio of flue gas (kg of water vapor/kg of dry flue gas)
v_{FG} mean superficial velocity of flue gas (m/s)
V_O volume of the internal oven chamber (m^3)
x'_i mass fraction of the generic ith element of wood on dry mass (g/g)
x_A ash content of firewood on wet matter (g/g)
x_M moisture content of firewood on wet matter (g/g)
$y_{i,FG}$ weight fraction of the ith component of flue gas
z_i characteristic dimension of the ith solid surface area (m)
0 initial
A referred to air
$\Delta \in_{CO_2}^{H_2O}$ binary overlap correction of the overall gas emissivity due to band overlapping of H_2O and CO_2 gases (dimensionless)
C referred to carbon
FG referred to flue gas
H referred to hydrogen
N referred to nitrogen
O referred to oxygen
S referred to sulfur
W referred to tray bottom

β_V volumetric coefficient of expansion of fluid (K^{-1})
ΔT temperature difference (= T_{Oi}—T_A) (°C)
ε_{CO_2} emissivity of carbon dioxide in the gas filling the oven chamber (dimensionless)
α_{FB} thermal diffusivity of firebrick (m^2/s)
$\alpha, \beta, \gamma, \delta$ stoichiometric coefficients of the wood combustion reaction (mol/mol)
ε_F emissivity of flame (dimensionless)
ε_G emissivity of flue gas (dimensionless)
ε_{H2O} emissivity of water vapor in the gas filling the oven chamber (dimensionless)
ε_i emissivity of the ith radiating surface area (dimensionless)
γ_{AS} ratio of the air-to-water convective heat transfer coefficients as defined by Equation (40) (dimensionless)
η_{comb} firewood combustion efficiency (dimensionless)
λ_e latent heat of water evaporation (J/kg)
μ_i dynamic viscosity of the ith fluid (kg/m/s)
ρ_i density of the ith fluid or solid ($kg\ m^{-3}$)
σ Stefan–Boltzmann constant (= $5.67 \times 10^{-8}\ Wm^{-2}\ K^{-4}$)

AUTHOR CONTRIBUTIONS

Aniello Falciano: Conceptualization; Validation; Investigation; Writing – review & editing. **Paolo Masi**: Conceptualization; Investigation; Validation; Writing – review & editing; Funding acquisition; Project administration. **Mauro Moresi**: Conceptualization; Investigation; Validation; Writing – original draft; Writing – review & editing; Methodology; Software.

ACKNOWLEDGMENTS

The authors would like to thank MV Napoli Forni Sas (Naples, Italy) and Kaleidostone Srl (Naples, Italy), for having, respectively, donated the wood-fired pizza oven and pizza counter used in this work, and Antimo Caputo Srl (Naples, Italy) for granting a Research Scholarship within the scope of this research. This research was funded by the Italian Ministry of Instruction, University and Research within the research project entitled The Neapolitan pizza: processing, distribution, innovation and environmental aspects, special grant PRIN 2017 - prot. 2017SFTX3Y_001.

Open Access Funding provided by Universita degli Studi della Tuscia within the CRUI-CARE Agreement.

CONFLICT OF INTEREST STATEMENT

The authors declare that they have no known conflict of interests or personal relationships that could have appeared to influence the work reported in this paper.

DATA AVAILABILITY STATEMENT

The datasets generated during and/or analyzed during the current study are available from the corresponding author on reasonable request.

ORCID

Aniello Falciano https://orcid.org/0000-0001-5924-3152
Mauro Moresi https://orcid.org/0000-0002-4706-0129

REFERENCES

Àgueda, A., Pastor, E., Pérez, Y., & Planas, E. (2010). Experimental study of the emissivity of flames resulting from the combustion of forest fuels. *International Journal of Thermal Sciences*, *49*(3), 543–554.

Alberti, M., Weber, R., & Mancini, M. (2018). Gray gas emissivities for H_2O-CO_2-CO-N_2 mixtures. *Journal of Quantitative Spectroscopy & Radiative Transfer*, *219*, 274–291.

Anon. (n.d.). *Emissivity table for infrared thermometer readings*. https://ennologic.com/wp-content/uploads/2018/07/Ultimate-Emissivity-Table.pdf (accessed on 11 March 2023)

Cimini, A., & Moresi, M. (2022). Environmental impact of the main household cooking systems - a survey. *Italian Journal of Food Science*, *34*(1), 86–113.

Carslaw, H. S., & Jaeger, J. C. (1959). *Conduction of heat in solids* (2nd ed.) (pp. 58–61). Clarendon Press.

Choi, Y., & Okos, M. R. (1986). Thermal properties of liquid foods: Review. In M. R. Okos (Ed.), *Physical and Chemical Properties of Food* (pp. 35–77). American Society of Agricultural Engineers.

Ciarmiello, M., & Morrone, B. (2016a). Numerical thermal analysis of an electric oven for Neapolitan pizzas. *International Journal of Heat and Technology*, *34*(2), S351–S358. https://doi.org/10.1828/ijht.34S223

Ciarmiello, M., & Morrone, B. (2016b). Why not using electric ovens for Neapolitan pizzas? A thermal analysis of a high temperature electric pizza oven. *Energy Procedia*, *101*, 1010–1017. https://doi.org/10.1016/j.egypro.2016.11.128

Earle, R. L., & Earle, M. D. (1983). *Unit operations in food processing* (Web ed.). The New Zealand Institute of Food Science & Technology (Inc.). https://www.nzifst.org.nz/resources/unitoperations/index.htm (accessed on 29 January 2023)

EC. (2010). European Commission Regulation (EU) No. 97/2010, entering a name in the register of traditional SPECIALITIES guaranteed [Pizza Napoletana (TSG)]. *Official Journal of the European Union*, *34*, 5. https://eur-lex.europa.eu/legal-content/EN/TXT/?uri=CELEX:32010R0097 (accessed on 29 January 2023)

EC. (2011). *European Commission, preparatory studies for eco-design requirements of EuPs (III): Lot 23 domestic and commercial hobs and grills, included when incorporated in cookers*. Final Version. https://www.eup-network.de/fileadmin/user_upload/Produktgruppen/Lots/Final_Documents/Lot_23_Task_3_Final.pdf (accessed on 29 January 2023)

Falciano, A., Masi, P., & Moresi, M. (2022). Performance characterization of a traditional wood-fired pizza oven. *Journal of Food Science*, *87*, 4107–4118. https://doi.org/10.1111/1750-3841.16268

Green, D. W., & Perry, R. H. (2008). *Perry's chemical engineers' handbook* (8th ed.). McGraw-Hill. https://doi.org/10.1036/0071422943

Hager, T. J., & Morawicki, R. (2013). Energy consumption during cooking in the residential sector of developed nations: A review. *Food Policy*, *40*, 54–63.

Heldman, D. R., & Lund, D. B. (2007). *Handbook of food engineering* (2nd ed.) (pp. 402–410). CRC Press, Taylor & Francis Group.

Henderson-Sellers, B. (1984). A new formula for latent heat of vaporization of water as a function of temperature. *Quarterly Journal of the Royal Meteorological Society*, *110*, 1186–1190.

Igo, S. W., Kokou, N., Compaoré, A., Kalifa, P., Sawadogo, G. L., & Namoano, D. (2020). Experimental analysis of the thermal performance of a metal fired-wood oven. *Iranian (Iranica) Journal of Energy and Environment*, *11*(3), 225–230.

Jones, J. M., Mason, P. E., & Williams, A. (2019). A compilation of data on the radiant emissivity of some materials at high temperatures. *Journal of the Energy Institute*, *92*, 523–534.

Kern, D. Q. (1950). *Process heat transfer* (pp. 82). McGraw-Hill Book Company, Inc..

Keyest, F. G., & Vines, R. G. (1964). The thermal conductivity of steam. *International Journal of Heat and Mass Transfer*, *7*, 33–40.

Manhiça, F. A. (2014). *Efficiency of a wood-fired bakery oven—Improvement by theoretical and practical* [PhD Thesis]. Chalmers University of Technology. https://research.chalmers.se/en/publication/203999 (accessed 29 January 2023)

Manhiça, F. A., Lucas, C., & Richards, T. (2012). Wood consumption and analysis of the bread baking process in wood-fired bakery ovens. *Applied Thermal Engineering*, *47*, 63–72.

Mukunda, H. S. (2009). *Understanding combustion* (2nd ed.). Orient Blackswan.

Neutrium. (2012). Properties of air. https://neutrium.net/properties/properties-of-air/ (accessed on 11 March 2023)

Ozgen, S., Cernuschi, S., & Caserini, S. (2021). An overview of nitrogen oxides emissions from biomass combustion for domestic heat production. *Renewable and Sustainable Energy Reviews*, *135*, 110113.

Singh, R. P., Erdoğdu, F., & Rahman, M. S. (2009). Specific heat and enthalpy of foods. In M. S. Rahman (Ed.), *Food properties handbook*. (2nd ed.) (pp. 517–543). CRC Press.

Engineering ToolBox. (2003). Water - Density, Specific Weight and Thermal Expansion Coefficients. https://www.engineeringtoolbox.com/water-density-specific-weight-d_595.html (accessed on 11 March 2023)

Varlamov, A., Glatz, A., & Grasso, S. (2018). The physics of baking good pizza. *Physics Education*, *53*(6), 065011. https://doi.org/10.1088/1361-6552/aadc2e

Vassilev, S. V., Baxter, D., Andersen, L. K., & Vassileva, C. G. (2010). An overview of the chemical composition of biomass. *Fuel*, *89*, 913–933.

Zhang, Y., Li, Q., & Zhou, H. (2016). *Theory and calculation of heat transfer in furnaces* (pp. 131–172). Elsevier. https://doi.org/10.1016/B978-0-12-800966-6.00011-9

How to cite this article: Falciano, A., Masi, P., & Moresi, M. (2023). Semiempirical modeling of a traditional wood-fired pizza oven in quasi-steady-state operating conditions. *Journal of Food Science*, *88,* 2036–2052. https://doi.org/10.1111/1750-3841.16532